A&A 372, 59–70 (2001)
DOI: 10.1051/0004-6361:20010487
© ESO 2001

Astronomy & Astrophysics

VLT-spectropolarimetry of the high-polarization Seyfert 1 galaxy Fairall 51⋆

H. M. Schmid[1,⋆⋆], I. Appenzeller[1], M. Camenzind[1], M. Dietrich[2], J. Heidt[1], H. Schild[3], and S. Wagner[1]

[1] Landessternwarte Heidelberg-Königstuhl, 69117 Heidelberg, Germany
[2] Dept. of Astronomy, University of Florida, 211 Bryant Space Science Center, Gainesville, FL 32611-2055, USA
[3] Institut für Astronomie, ETH Zentrum, 8092 Zürich, Switzerland

Received 20 December 2000 / Accepted 22 March 2001

Abstract. We present high-precision optical spectropolarimetry of the Seyfert 1 galaxy Fairall 51 (F51) taken with FORS1 at the VLT. The observed spectrum shows unpolarized and linearly polarized components. The AGN continuum and the broad lines show (after correction for the Galactic interstellar polarization and the light contribution of the F51 host galaxy) a practically identical amount of intrinsic polarization ranging from 5% in the red to 13% in the UV. The narrow lines are unpolarized or show only little intrinsic polarization. The observed AGN continuum and the broad line radiation can be explained by a combination of reddened (and attenuated) direct light and scattered light reflected from an optically thin dust region. Hence, within the framework of the unification scheme of AGN, the Seyfert 1 galaxy F51 appears to be an example of a borderline Seyfert 1/Seyfert 2 case where the nucleus is partially obscured like for other type 1 AGN with high intrinsic scattering polarization. It is found that the scattering region in F51 is located far from the BLR and the continuum source. Thanks to this special scattering configuration, we were able to study the kinematics (line profiles) of the broad line region from two different viewing angles, one along the line of sight (in total light) and one via the scattering region (in polarized light). The line profiles in polarized and total light are found to be indistinguishable to a very high accuracy, strongly indicating that the velocity field of the F51 BLR is essentially spherically symmetric.

Key words. galaxies: active – galaxies: Seyfert – galaxies: individual: F 51 – polarization – scattering

1. Introduction

Seyfert galaxies often show intrinsic optical linear polarization (Martin et al. 1983; Brindle et al. 1990a). This polarization can be produced by scattering of the emission from the nucleus, of the broad line region (BLR), or of the narrow line region (NLR) by dust particles or electrons in an asymmetric geometry. Another effect producing polarization is ("dichroic") absorption due to aligned dust grains in the host galaxy. Furthermore, active galactic nuclei (AGN) with significant radio-emission may also emit polarized optical synchrotron radiation (e.g. Angel & Stockman 1980).

One of the major advances in the research of AGN was the finding that Seyfert 2 galaxies often show prominent Seyfert 1 characteristics (like broad emission lines) in polarized light. This indicates that at least some of the type 2 Seyfert nuclei are in fact partially obscured type 1s, a result which provided the key for the unification of Seyfert galaxies and other classes of AGN (Antonucci & Miller 1985; Miller & Goodrich 1990; Antonucci 1993; Cohen et al. 1999).

On the other hand, there exist also classical Seyfert 1 galaxies with strongly polarized BLR and continuum emission. An example is the Seyfert 1 galaxy Fairall 51, where high polarization had been noticed already by Martin et al. (1983), Thompson & Martin (1988) and Brindle (1990a, 1990b). As F51 is a radio-quiet object, synchrotron emission can be neglected as contribution to the polarization spectrum. The high polarization, therefore, indicates that a substantial fraction of the observed light is scattered by dust or free electrons in the system.

In order to investigate the origin of the polarization of F51 and the geometry of the system we carried out spectropolarimetry with a high signal-to-noise ratio using the VLT and FORS1. In this paper we report the results

Send offprint requests to: H. M. Schmid,
e-mail: hschmid@astro.phys.ethz.ch

⋆ Based on observations obtained at the ESO VLT UT1 (Antu) at Cerro Paranal, Chile (ESO program 63.P-0074).

⋆⋆ *Present address:* Institut für Astronomie, ETH Zentrum, 8092 Zürich, Switzerland.

Article published by EDP Sciences and available at http://www.aanda.org or http://dx.doi.org/10.1051/0004-6361:20010487

Table 1. F51 observing log; Res. is the nominal resolution for a slit width of 0.8″ and $t_{\rm exp}$ the exposure time of an entire cycle of four observations.

grism	λ-range [Å]	Res. [Å]	date 1999	$\rm UT_{start}$ hh:mm	$t_{\rm exp}$ min
G600R	5400–7500	4.2	Aug. 21	00:06	20
				00:35	80
				02:06	80
G600B	3600–6000	4.7	Aug. 22	01:25	60
				02:37	60
				03:50	40
G600I	7000–9200	4.2	Aug. 22	04:42[a]	60

a: Relatively large airmass of 1.5 − 1.8.

of these observations. A preliminary report of this work and of observations of other Seyfert 1 galaxies is given in Schmid et al. (2000).

2. Observations

Optical spectropolarimetry of F51 was performed during the two nights of August 21 and 22, 1999 with FORS1 at the ESO VLT Unit Telescope UT 1 (Antu). FORS1 is a multi-mode focal reducer imager and grism spectrograph equipped with a Wollaston prism and rotatable retarder plate mosaics in the parallel beam allowing linear and circular polarimetry and spectropolarimetry (Appenzeller et al. 1998).

We obtained three complete sets of polarization frames with the G600R and the G600B grisms. An additional set with the G600I grism was taken to extend the wavelength coverage towards the near infrared. A log of the observations is given in Table 1. With a slit width of 0.8″ we obtained a ($FWHM$) spectral resolution of ∼4.5 Å (see Table 1) corresponding to a velocity resolution of about 200 km s^{-1} near Hα and 350 km s^{-1} around 4000 Å. The seeing for these observations was around 0.8″ in both nights.

The linear polarization was measured in a standard way (e.g. Tinbergen & Rutten 1997) with sets of four observations taken at half-wave plate position angles of 0°, 22.5°, 45°, 67.5°, respectively. The data were recorded with a 2k × 2k CCD with a pixel scale of 0.2″/pixel in spatial and 1 Å/pixel in spectral direction.

In addition to the Seyfert 1 galaxies we observed polarized (HD 126593, BD+25°727) and unpolarized (HD 176425, BD+28°2411) standard stars for checking and correcting the instrumental effects. As not enough good observations of the unpolarized standard stars could be obtained, the telescope instrumental polarization at the time of the observations (of the order 0.1%) could not be determined well. Therefore, a systematic error of $\Delta p \approx 0.15\%$, $\Delta\theta \approx 2°$ may be present in our polarization data. In view of the observed polarization effects of 5% to 12% this potential error has no effect on our conclusions, but its presence has to be taken into account when comparing our data to other precise polarization measurements. The photon noise errors are generally below $\Delta p = 0.1\%$.

Because of a reflex image from the FORS optics in our G600B data, the wavelength region from 4000 to 4100 Å (marked in Fig. 1) was not used in our analysis. The reflex is known to occur for this special Grism/Wollaston configuration.

BD+28°2411 is also a spectrophotometric standard star and was observed with a wide slit (5″) for the calibration of the intensity spectrum. This calibration was applied to the F51 spectra, but no correction for the (substantial) slit losses at the 0.8″ wide and 8″ long slit aperture was made. Nonetheless, we obtained a very good match (better than 5%) in the overlap region of the G600B and G600R flux spectra, indicating that the relative energy distribution (colour calibration) for the nuclear spectrum of F51 is accurate. The flux scale of the G600I spectrum turned out to be about 10% lower compared to the G600R spectrum. This can be explained by a small pointing offset. We therefore adjusted the flux of the G600I spectrum to the G600R scale.

3. Spectroscopic properties of the F51 nucleus

3.1. Basic properties

The F51 host galaxy is a bared spiral (SBb) with a redshift of 0.01419. The bar extends to about 15″ (∼5 kpc) on both sides of the nucleus in north-south direction (West et al. 1978; Malkan et al. 1998). The 20″-long slit was placed along the bar and the spectrum of the core was extracted from a 8″-wide strip. From the remaining slit region the spectrum of the host galaxy was obtained.

Because of the long integration time required for spectropolarimetry we obtained as a byproduct very high S/N intensity spectra of F51 (see Fig. 1). The core spectrum of F51 shows a rather flat continuum (in F_λ) and the typical BLR lines of H I, He I and Fe II with widths of about 3000 ± 1000 km s^{-1} ($FWHM$). In addition, the spectrum displays strong NLR emissions of H I, [N II], [O III] etc., and forbidden high-excitation lines such as [Fe VII] and [Fe X]. Observed flux values (uncorrected for slit losses) for the narrow lines, the broad lines, and 200 Å-wide "continuum" intervals are given in Tables 2–4, respectively.

The observed continuum flux of our spectra is about a factor of two lower than published spectrophotometry of Morris & Ward (1988) and Winkler (1992). For the narrow line flux of [O II] and [S II], the factor is even larger (∼3.5). At least part of this apparent discrepancy is due to light losses at the 0.8″ slit used in our observation in order to keep the spectral resolution high. The narrow low-excitation lines [N II] and [S II] are expected to originate from a more extended region, which explains their relative weakness in our spectra compared to previous observations taken with much wider slits. From the

Table 2. Narrow emission line parameters. Observed flux $f_{\rm obs}$ (in units of 10^{-15} erg/s cm^2) and polarization $p_{\rm obs}$ and $\theta_{\rm obs}$. Upper $p_{\rm obs}$-limits are given for stronger lines without a significant polarization detection.

$\lambda_{\rm obs}$ [Å]	line	$f_{\rm obs}$ [10^{-15}]	$p_{\rm obs}$ [%]	$\theta_{\rm obs}$ [°]
3780.6	[O II]	13.0	<4	
3810.6	[Fe VII]	2.6		
3923.5	[Ne III]	10.1	<4	
3944.6	H8	2.0		
4024.4	[Ne III]	2.8		
4126.8	[S II]	0.7		
4160.0	Hδ	1.5		
4402.0	Hγ	3.3		
4424.9	[O III]	1.4		
4751.0	He II	4.3	<4	
4929.9	Hβ	9.4	<2	
5028.5	[O III]	38.0	1.3 ± 0.2^a	-27 ± 4^a
5077.1	[O III]	123.	1.4 ± 0.1^a	-31 ± 2^a
5800.1	[Fe VII]	3.3	<4	
5959.0	He I	1.5		
6169.8	[Fe VII]	7.5	<3	
6390^b	[O I]	3.6		
6400^b	[S III]	0.6		
6455^b	[O I]	1.7		
6462^b	[Fe X]	1.3		
6641.2	[N II]	10.1	<3	
6655.7	Hα	42.1	<1.5	
6676.9	[N II]	24.7	<2	
6811.7	[S II]	10.1	<2	
6826.4	[S II]	10.2	<2	
7237.2	[Ar III]	1.6		
7423^b	[O II]	1.3		
7433^b	[O II]	1.1		

a: The [O III] line polarizations after correction for the Galactic interstellar polarization are:
$p_{\rm corr} = 1.1 \pm 0.3\%$, $\theta_{\rm corr} = -51° \pm 8°$ for [O III] at 5028 Å
$p_{\rm corr} = 1.3 \pm 0.2\%$, $\theta_{\rm corr} = -53° \pm 4°$ for [O III] at 5077 Å.
b: Line center measurement affected by nearby line.

published spectral plots (Morris & Ward 1988; Winkler 1992) we infer that the continuum flux distribution F_λ from 3800–9000 Å is practically flat to an accuracy of about 15%. Our data yield the same result, confirming our relative photometric calibration.

Nebular line analysis yields for the NLR an electron density of $N_{\rm e} = 600$ cm^{-3} from the [S II] doublet ratio $F(\lambda6716)/F(\lambda6731)$ and an electron temperature of $T_{\rm e} = 15000$ K from the [O III] ratio $F(\lambda5007)/F(\lambda4363)$ (dereddened by $E_{B-V} = 0.6$, see below).

Stellar and interstellar absorptions from the host galaxy are clearly visible in the core spectrum for the Ca II K and Na I resonance lines and the Ca II triplet near 8600 Å. These lines can be recognized because they fall into spectral regions with not too strong nuclear emission features.

3.2. Reddening of the NLR-spectrum

The narrow line fluxes indicate substantial dust reddening. Assuming case B recombination theory for the Balmer lines yields $E_{B-V} = 0.41$ and 0.66 for the line ratios Hα/Hβ and Hγ/Hβ, respectively. Alternatively, a reddening of $E_{B-V} = 0.65$ is derived from the combination of [S II] and [O II] line ratios (Allen 1979). The accuracy of the different extinction measurements is discussed in detail in e.g. Malkan (1983) and Tsvetanov & Yancoulova (1989). The conclusion is that the S II–O II-method and the Hγ/Hβ-ratios seem to be the most reliable, while the Hα/Hβ-ratio may be disturbed by various effects. According to Tsvetanov & Yancoulova (1989) the S II–O II-value should be corrected by about -0.08 mag to account for density inhomogeneities in the NLR. Therefore we adopt here a value of $E_{B-V} = 0.60$ for the reddening of the NLR-spectrum.

That the nucleus of F51 is substantially reddened was also noticed by Winkler (1997) in a study of the colours of the variable nuclear component. He found a nuclear reddening of $E_{B-V} = 0.58$ based on the assumption that the nuclear variations are grey and the intrinsic nuclear colours of F51 are equal to unobscured Seyfert 1 objects like Mrk 509 or Ark 120.

Due to the intermediate Galactic latitude $b = -23.1°$ of F51 Galactic reddening cannot be neglected. This contribution can be estimated from the maps of IR dust emission (Schlegel et al. 1998/NED database), which indicate $E_{B-V} = 0.11$. Alternatively, we can use foreground stars as probes of the Galactic extinction towards F51. The bright Be star λ Pav, located only 38′ east and 10′ north of F51 is extremely well suited to this purpose. Already existing extinction values for λ Pav are $E_{B-V} = 0.09$ or 0.10 and a distance of 400 pc (Jenkins 1978; Zorec & Briot 1991). Thus, we attribute a reddening of $E_{B-V} = 0.10$ in the F51 spectrum to the dust in the Milky Way disk.

Comparing this value with the total reddening derived above indicates that extinction by dust in the host galaxy is the main cause of the reddening, while dust in the Milky Way contributes to a lesser extent.

4. The polarized spectrum

4.1. Observed polarization properties

The solid curves in Figs. 1 and 2 represent the spectropolarimetric results obtained for F51.

The observed linear polarization $p_{\rm obs}$ and position angles $\theta_{\rm obs}$ for the narrow lines, for the broad lines, and for continuum intervals are listed in the Tables 2–4, respectively. The main results can be summarized as follows:

– The observed linear polarization $p_{\rm obs}$ in the continuum rises from about 3% at 8500 Å to 11% at 3700 Å. This rise has been reported by Martin et al. (1983) and Thompson & Martin (1988) on the basis of multifilter polarimetry taken in April 1980. Compared to

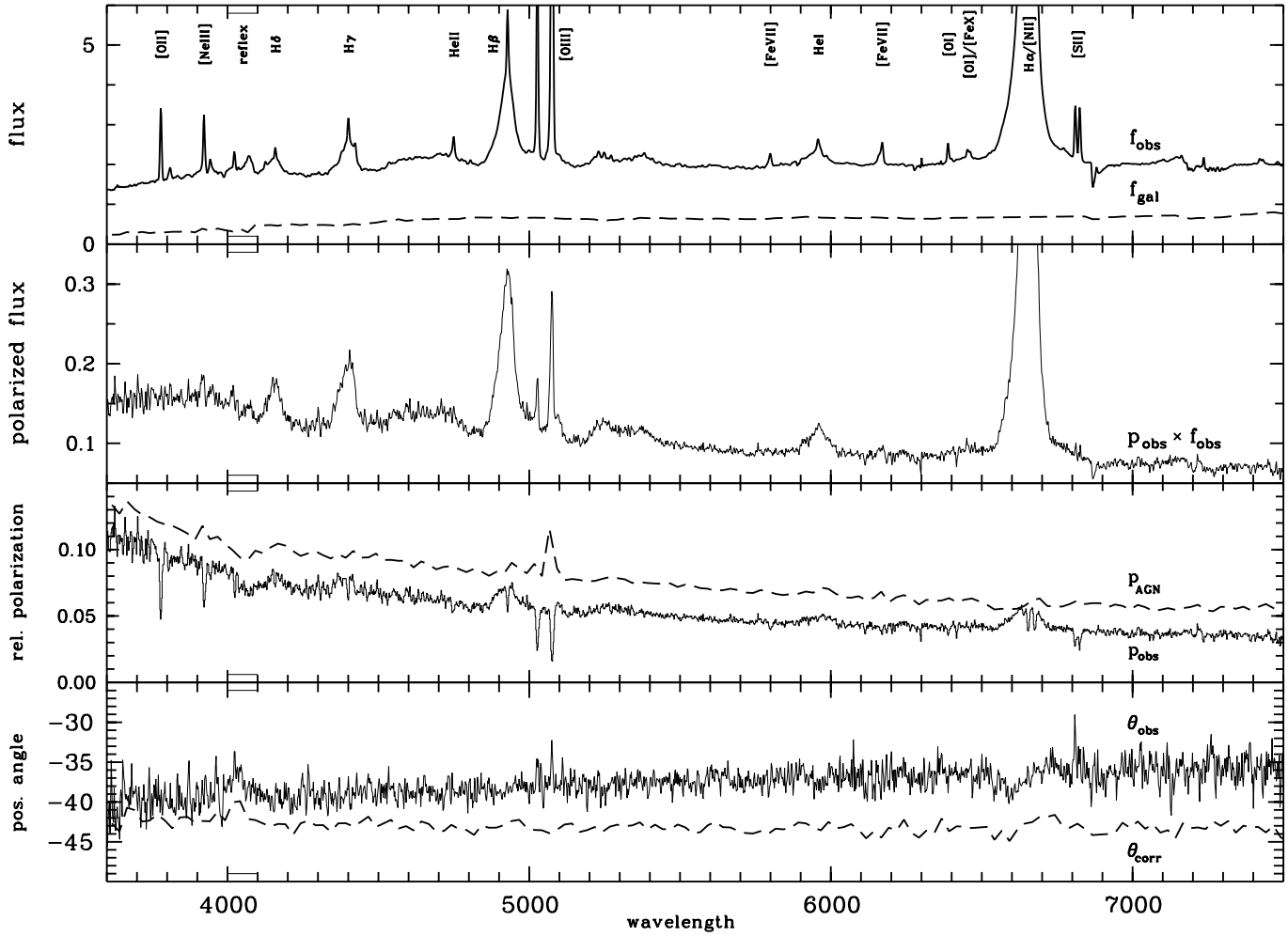

Fig. 1. VLT-spectropolarimetry of F51. The top panel gives the flux spectrum $f_{\rm obs}$ in units of 10^{-15}erg/s cm^2 Å of the bright core (solid) and the scaled spectrum from the bar of the host galaxy $f_{\rm gal}$ (dashed). The polarized flux spectrum $p_{\rm obs} \times f_{\rm obs}$ is plotted in the second panel. The third panel shows the relative linear polarization $p_{\rm obs}$ and the relative polarization of the active nucleus $p_{\rm agn} = p \times f/f_{\rm agn}$ corrected for the Galactic interstellar polarization. The spectrum from the active nucleus $f_{\rm agn}$ is the top spectrum $f_{\rm obs}$ with the narrow lines and the galaxy spectrum $f_{\rm gal}$ subtracted. The solid curve in the bottom panel is the measured polarization position angle, while the dashed curve is the binned position angle intrinsic to F51 after correction for the Galactic interstellar polarization. The short lines from 4000 Å to 4100 Å mark the region contaminated by the reflex described in Sect. 2.

the total flux, the colours of the polarized flux $p \times f$ are significantly bluer by about $B - V = 0.35$ mag;

– The broad H I and He I λ5876 lines and the broad Fe II feature at λ5200 show a higher relative polarization $p_{\rm obs}$ than the adjacent continuum. The polarization of the Balmer lines Hα, Hβ, Hγ, and Hδ shows roughly the same wavelength dependence as the continuum, but at a level which is about 1.6 times higher;

– The line structure of the broad Hα and Hβ lines are practically identical in total and polarized light (Fig. 2). Even subtle structural features like the more extended blue wing are in very good agreement between the total and the polarized flux profiles;
A very small deviation of $\Delta\theta = -1.5°$ to $+1.5°$ is visible in Fig. 1 in the position angle across the Hα line profile. This feature can be explained by a second polarization component of $p \approx 0.3\%$ in the Hα line wings with a position angle of roughly $-80°$ in the blue wing and $+10°$ in the red wing. This small line wing polarization component is more than an order of magnitude smaller than the main polarization component of $p = 5.6\%$ at $\theta = -37.2°$ in Hα (Table 3) and only visible due to the very high quality of our data;

– The narrow [O III] lines show (as observed first by Brindle et al. 1990b) little polarized flux with a total linear polarization of about 1.4% only. All other narrow lines from low and highly ionized atoms are hardly visible in the polarized flux spectrum. Their intrinsic polarization is below the upper limits given in Table 2. In all cases the narrow line polarization is much lower than the polarization in the continuum or the broad lines;

– The amount and position angle of the observed continuum polarization are within the various error limits,

Table 3. Broad line parameters. Observed flux $f_{\rm obs}$ and polarization $p_{\rm obs}$ and $\theta_{\rm obs}$. The contribution of the Galactic interstellar polarization has been vector-subtracted for $p_{\rm corr}$ and $\theta_{\rm corr}$. The measuring errors are the same for observed and corrected values. The fluxes (in units of 10^{-15} erg/s cm^2) refer to a small aperture with significant seeing losses (see Sect. 3.1).

line	$f_{\rm obs}$	$p_{\rm obs}$ [%]	$\theta_{\rm obs}$ [°]	$p_{\rm corr}$ [%]	$\theta_{\rm corr}$ [°]	errors [%/°]
Hδ	16.8	12.0	−42.3	12.0	−44.8	2.4/5.7
Hγ	44.3	9.2	−39.3	9.1	−42.6	0.7/2.2
Fe II 4570	63.3	5.8	−37.4	5.6	−42.6	1.6/8.9
Hβ	143.	8.5	−38.3	8.3	−41.8	0.6/2.0
Fe II 5200	44.6	7.1	−37.7	7.3	−42.2	1.1/4.4
He I 5876	24.7	8.8	−36.9	8.7	−40.5	1.6/5.2
Hα	753.	5.8	−37.2	5.6	−42.5	0.2/1.0
O I 8446	24.5	4.8	−40.4	5.3	−45.2	2.0/11.3

identical to the values reported in the earlier papers quoted above. Hence there is no evidence for any time variation of the polarization during the past 20 years.

The polarization parameters $p_{\rm obs}$ and $\theta_{\rm obs}$ in Tables 2–4 were calculated from the Stokes Q and U spectra according to $p = (Q^2+U^2)^{1/2}/f$, where f is identical to Stokes I, and $\theta = 0.5\arctan(U/Q)$.

The errors for the continuum polarization listed in Table 4 are dominated by the error introduced by the inaccurate derivation of the instrumental polarization and are about 0.15% for p and 2° for θ. The accuracy of the polarization of the broad lines (Table 3) is mainly due to uncertainties in the continuum definition. The errors are, therefore, larger for weaker lines and the broad Fe II features. The spectral resolution of our data is sufficiently high to correct accurately for the narrow line emission in the flux spectrum. The continuum level in the $Q-$, $U-$, and f-spectra was defined by a straight line between two line free intervals on both sides of the broad line. The polarization of the narrow [O III] lines can be determined with high accuracy. More difficult is a polarization measurement in the narrow Hα component. A weak signal seems to be present in the Stokes Q spectrum. But no significant measurement was possible due to uncertainties in defining the underlying broad component and [N II] features. The upper limits given for the other narrow lines are 3 σ-values that take into account the photon statistics for the narrow line and the noise level in the adjacent spectral region (continuum, broad lines).

4.2. Interstellar polarization

4.2.1. Polarization by dust in the Milky Way

Some information on the Galactic interstellar polarization along the line of sight towards F51 has been obtained by simultaneous measurements of a field star (star #6 of the F51 photometric sequence of Hamuy & Maza (1989)) which was in slit #16 of the polarimetric focal plane mask

Table 4. Measured mean flux and polarization of F51 for broad wavelength intervals. The observed flux $f_{\rm obs}$ and the flux for the active nucleus are given in 10^{-15} erg/(s cm^2 Å). $p_{\rm obs}$ and $\theta_{\rm obs}$ are flux weighted means of the polarization parameters. The flux and polarization of the active nucleus $f_{\rm agn}$, $p_{\rm agn}$ and $\theta_{\rm agn}$ are derived after correction for the Galactic interstellar polarization and the dilution by the host galaxy. Errors are dominated by the uncertainties in the instrument calibration and the correction procedures. Note that the fluxes refer to a small aperture with significant seeing losses (see Sect. 3.1).

interval $\lambda\lambda$	$f_{\rm obs}$	$p_{\rm obs}$ [%]	$\theta_{\rm obs}$ [°]	$f_{\rm agn}$	$p_{\rm agn}$ [%]	$\theta_{\rm agn}$ [°]
3600–3800	1.56	10.0	−39.9	1.22	12.7	−42.3
3800–4000	1.83	8.7	−39.4	1.42	11.0	−42.3
4000–4200[a]						
4200–4400	1.88	7.2	−39.3	1.40	9.5	−43.0
4400–4800	2.13	6.5	−38.7	1.53	8.8	−43.0
4800–5200[b]	2.86	5.3	−38.0	1.78	8.2	−43.5
5200–5600	2.08	5.2	−37.7	1.44	7.3	−43.2
5600–6000	2.04	4.7	−36.9	1.38	6.6	−43.3
6000–6400	2.03	4.2	−36.7	1.35	6.1	−43.5
6400–6800[c]	4.17	4.6	−37.0	3.27	5.7	−43.1
6800–7200	2.07	3.7	−36.0	1.33	5.4	−43.4
7200–7600[d]	1.94	3.2	−35.6	1.22	5.0	−43.7
7600–8000[d]	1.76	2.8	−37.0	1.09	4.5	−46.0
8000–8400[d]	1.77	2.9	−35.5	1.10	4.4	−43.9
8400–8800	1.88	2.9	−35.4	1.21	4.3	−43.3
8800–9100[d]	1.60	2.6	−34.6	0.98	4.0	−43.1

a: Affected by reflected light.
b: Includes the strong Hβ and [O III] emission lines.
c: Includes the strong Hα line.
d: Includes strong telluric absorption, which are not corrected for the $f_{\rm obs}$ and $f_{\rm agn}$ values.

formed by the FORS MOS unit. For this object we obtained a polarization of $p = 1.0 \pm 0.2\%$, $\theta = 0° \pm 5°$ for the $\lambda\lambda 5500 - 7500$ range. According to our spectrum this star has a spectral type of G8 in agreement with the colours of Hamuy & Maza (1989) and an estimated Galactic reddening of $E_{B-V} = 0.10$ (Sect. 3.1). Assuming that this is a G8 V dwarf with $m_V = 15.6$ it is located at a distance of roughly 1 kpc, far enough to probe the entire interstellar polarization in the Galactic plane.

Unfortunately, we found no really suitable nearby object in the literature to cross-check our interstellar polarization determination. The close (40′ away) Be star λ Pav is known to have a variable intrinsic polarization (Serkowski 1970). However, the Galactic polarization maps of Mathewson & Ford (1970) and the corresponding catalogues (Mathewson et al. 1978) for stellar polarization data indicate that the interstellar polarization in the region of F51 is rather homogeneous on relatively large scales. Therefore, it seems likely that HD 167128, which is 7° away from F51 still has a similar interstellar polarization. The polarization of this star $p = 0.98$ %, $\theta = 3°$ agrees well with star 6 in the F51 field and therefore

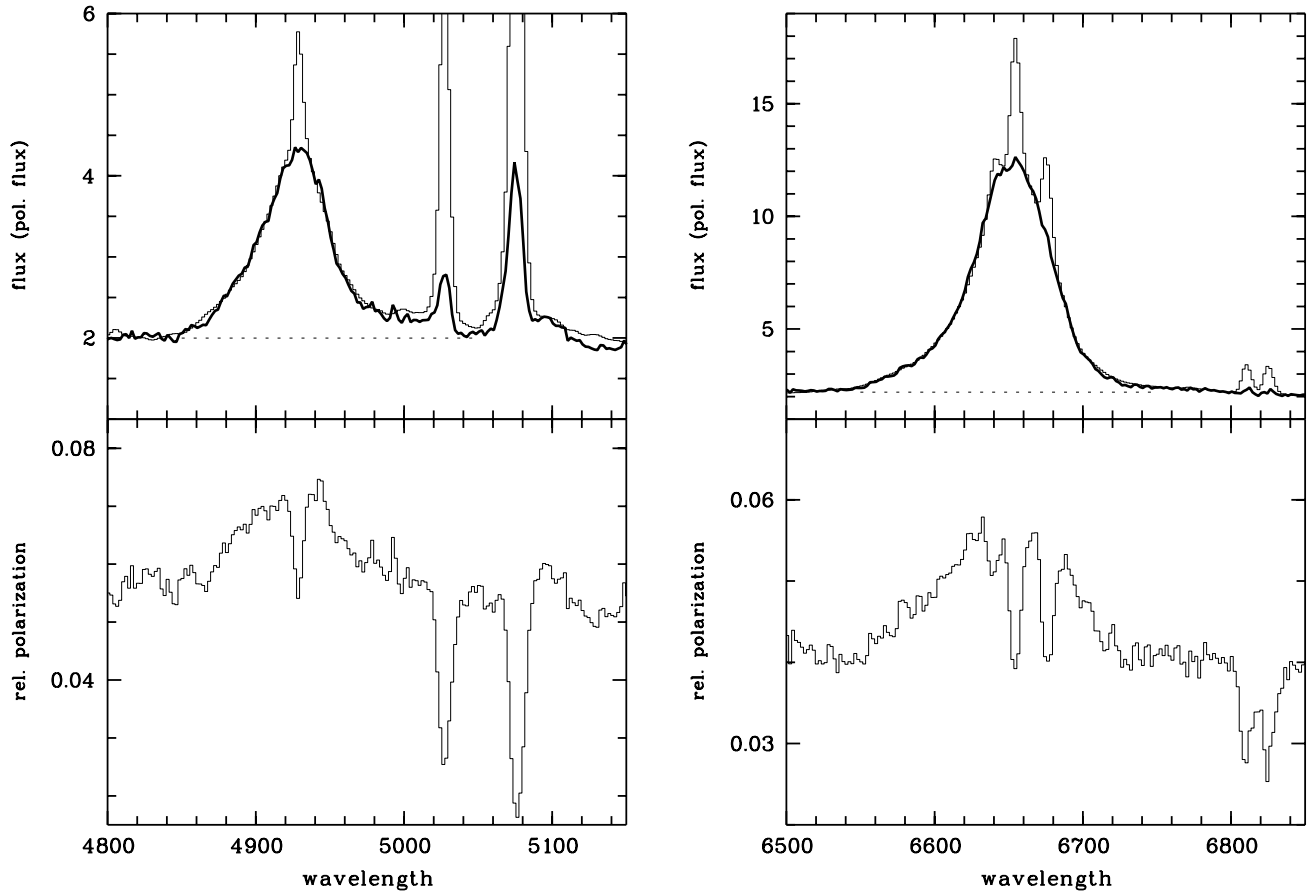

Fig. 2. Observed polarization of the Hβ/[O III] and the Hα-region of F51. Upper panel: Comparison of the Hβ and Hα broad line profiles in the flux (thin line and flux scale) and polarized flux spectrum (thick line). The dotted line indicates the level of zero line flux (continuum level) for both the f and the $p \times f$ spectrum. For comparison purposes the $p \times f$-profiles are normalized to the f-profiles for the broad lines. The similarity between f and $p \times f$ shows that the structures of the broad Hα and Hβ components are essentially identical in polarized and total light. Lower panel: the observed linear polarization.

provides some independent support (despite the large separation) that the Galactic interstellar polarization derived from star # 6 is correct for F51. Therefore, we correct our F51 measurements for Galactic interstellar polarization by subtracting the relative Stokes parameters of star # 6, assuming a Serkowski law (Serkowski et al. 1975) with $p_{\max} = 1$ %, $\lambda_{\max} = 5500$ Å and $\theta = 0°$.

Applying this correction to the F51 data strongly reduces the angle rotation from blue to red. In fact, the observed rotation from blue to red of $\Delta\theta = +4°$ in the continuum polarization disappears to $|\Delta\theta| < 1°$ (see $\theta_{\rm AGN}$ in Table 4 and Fig. 1). Such a behaviour is expected if an interstellar correction is applied to a polarized source with one predominant polarization angle. This can therefore be considered as further support for the adopted Galactic interstellar polarization. The position angle of the corrected polarization is close to $-43°$ for both the broad lines and the continuum (Tables 3, 4). The amount of polarization p is hardly affected by the Galactic interstellar correction as can be seen from $p_{\rm obs}$ and $p_{\rm corr}$ in Table 3. Note that $p_{\rm AGN}$ in Table 4 includes also a correction for the light contamination by the host galaxy.

4.2.2. Interstellar polarization in the host galaxy

As pointed out in Sect. 3.2, most of the substantial reddening of $E_{B-V} \approx 0.6$ mag derived for the narrow-line spectrum must be due to dust absorption in the host galaxy. Hence we have to investigate whether dichroic dust absorption in the host galaxy introduces another polarization component. In view of the moderate inclination angle of F51, the dust absorption certainly does not occur in a spiral arm, as in the case of interstellar extinction and polarization in the solar neighborhood. Therefore it is difficult to predict how much polarization one should expect on the basis of the observed reddening.

An upper limit for the interstellar polarization in the host galaxy can be estimated from the polarization of the narrow emission lines. As listed in Table 2 (and its footnote) the polarization of the [O III] lines (corrected for the Galactic interstellar polarization) is about 1.2% . For the other (much weaker) narrow lines no statistically significant results could be obtained. But, as illustrated in Figs. 1 and 2, some narrow lines (e.g. the weak [S II] doublet) show a weak signal in polarized flux. For all these lines the amount of polarized flux (and the amount of

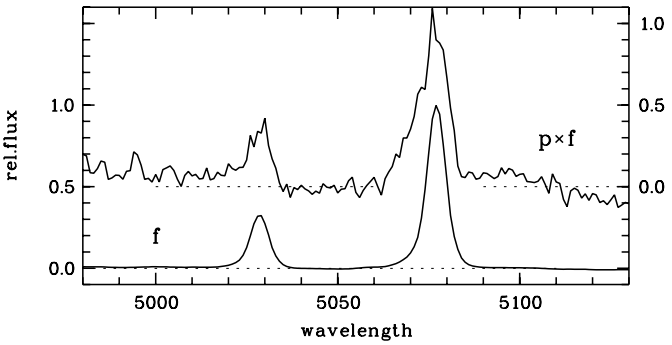

Fig. 3. Profiles of the narrow [O III] lines in total and polarized flux. Note the more extended blue wings in the polarized flux profile. Both spectra are scaled and shifted such that the continuum between the two lines is zero and the peak of the $\lambda_0 = 5007$ Å transition at 5077 Å is equal to one.

polarization) is within the error limits well compatible with the assumption that all narrow lines (including the narrow components of the Balmer lines) show the same intrinsic polarization as the [O III] lines. Therefore, we cannot rule out that some of the small polarization observed in [O III] and the other narrow lines is indeed produced by dichroic absorption and forward scattering by aligned dust grains in the host galaxy.

On the other hand, from Fig. 3 we see that the [O III] line profiles differ significantly between the intensity (flux) spectrum and the polarized flux spectrum. At least the stronger [O III] line shows an extended blue wing in $p \times f$ that is not present in f. A similar extension can be seen in the weaker [O III] line although the signal is comparable to the noise level. Such a line profile change cannot be produced by absorbing or forward scattering dust. Therefore, we regard it as more likely that interstellar polarization in the host galaxy is negligible and that the polarization in the [O III] lines is caused by scattering of line photons in an asymmetric scattering geometry. The fact that the polarized line profile extends towards the blue would further indicate that the corresponding scattering region is moving toward the [O III] emittion gas. We strongly favour this possibility and therefore make no correction for interstellar polarization in the host galaxy.

We note that even if all the polarization observed in [O III] should in fact be due to host galaxy interstellar polarization, neglecting this component would have practically no effect on our analysis. This is because the [O III] polarization is much smaller than the continuum and BLR polarization and the position angles of this component is (in contrast to the Galactic interstellar component) almost identical to that of the intrinsic continuum and BLR polarization.

4.3. The AGN spectrum and the dilution by the host galaxy

For the interpretation of the scattering polarization it is essential to separate the emission from the active nucleus, the host galaxy and the narrow line region according to $f_{\rm AGN} = f_{\rm obs} - f_{\rm NLR} - f_{\rm gal}$. The narrow lines are well defined in our data and can be accurately separated from broad lines and continuum. The separation of the spectra of the host galaxy $f_{\rm gal}$ and the active nucleus $f_{\rm AGN}$ is more difficult.

An estimate of the host galaxy flux can be obtained from the strength of the Ca II triplet absorptions $\lambda\lambda$8498, 8542, 8662 Å. Terlevich et al. (1990) studied the strengths of the Ca II triplet lines in the nuclear region of normal and active galaxies. They found that the equivalent widths of the Ca II lines show only a small spread of about ±1 Å around a mean value of 7 Å. This result is largely independent of the nucleus type, such as LINER, starburst or Seyfert 2. Following their recipe, we measure 2.1 ± 0.6 Å for the Ca II triplet equivalent width in F51. From this we can conclude that the host galaxy of F51 contributes about 30% to the total spectrum in this wavelength region. As F51 is a Seyfert 1 galaxy where peculiar line emission from the H I Paschen series and the Ca II triplet cannot be excluded, it is difficult to make a statement about the accuracy of this estimate.

To obtain a template which would allow correcting for the host galaxy flux, we observed the spectrum of the bar region of F51. This spectrum was recorded on both sides of the 8″ wide core region. The spectrum contains the typical stellar absorptions of galaxies, emission lines from H II regions and some contamination from scattered light and the seeing halo of the very strong Hα emission of the F51 core. Emission lines and the Hα contamination were clipped and the resulting spectrum smoothed. This "host galaxy spectrum" was then normalized in order to match the expected contribution of stellar light in the core region and subtracted from the observed spectrum of the core.

Interestingly, we find that the resulting relative polarization spectrum of the active nucleus $p_{\rm AGN} = p_{\rm corr} \times f_{\rm obs}/f_{\rm AGN}$ (see below) becomes practically featureless, i.e. the BLR features disappear in the $p_{\rm AGN}$-spectrum since continuum and lines now show the same polarization. The smoothest $p_{\rm AGN}(\lambda)$-spectrum is obtained for a host galaxy contribution of 35–40% to the total continuum near the Ca II triplet.

Such a behaviour (i.e. broad lines and continuum showing the same polarization) is expected if the nuclear continuum and the emission of the BLR are scattered by the same medium and have the same scattering geometry. This would be fulfilled in cases where the distance to the main scattering region is much larger than the size of the continuum and broad line region.

Thus, it seems warranted to improve the rough estimate on the host galaxy contribution from the Ca II lines using the smoothness of the resulting polarization spectrum $p_{\rm AGN}$. Based on this, we adopt in the following that the host galaxy contributes 38% of the light of the observed core spectrum at the wavelength of the Ca II triplet. The corresponding smoothed $f_{\rm gal}$ spectrum is plotted in Fig. 1.

The AGN spectrum $f_{\rm AGN}$ obtained by subtracting the host galaxy is plotted in Fig. 4. The relative polarization corrected for the interstellar polarization and the dilution by the host galaxy and the narrow lines was derived according to

$$p_{\rm AGN} = p_{\rm corr} \times f_{\rm obs}/f_{\rm AGN}$$

and plotted in Fig. 1. In general, such procedures have to be carried out for the corresponding Stokes parameters. However, assuming that the polarization of the host galaxy spectrum can (like that of the narrow emission lines) be neglected relative to the polarization of the AGN spectrum, the calculation can be made directly with the relative polarization spectrum p. This is an acceptable assumption given the absence of a significant intrinsic position angle rotation in the continuum and the small intrinsic polarization in the narrow lines. Only at the position of the very strong [O III] lines do we see a spurious feature in the $p_{\rm AGN}$ spectrum due to the intrinsic narrow line polarization. The relative polarization spectrum $p_{\rm AGN}$ obtained with the procedure described above is practically featureless apart from a smooth slope from $p_{\rm agn} = 12.7\%$ at 3700 Å to $p_{\rm agn} = 4.3\%$ around 8500 Å (Table 2).

We note that this result depends on the assumed strength and colour of the host galaxy contribution. An error in the derivation of the host galaxy contribution by a factor of 1.3 would increase or decrease $p_{\rm agn}$ by about ± 0.4 to $\pm 0.8\%$ in the red and the blue respectively. Moreover, we have assumed that the spectrum of the stellar populations in the bar and core region of F51 have a similar spectral distribution. This must not be true given the possibility that there could be different stellar populations and, in particular, different dust reddening. However, the spectral slope of the host galaxy contribution must deviate very strongly from the adopted one to put our result of a practically featureless polarization spectrum $p_{\rm agn}$ into question.

5. Direct and scattered radiation from the active nucleus

5.1. Assumptions and simplifications

A straightforward explanation for the observed high polarization of the AGN radiation is the assumption that the observed flux of the active nucleus $f_{\rm AGN}(\lambda)$ is composed of two components, the direct nuclear light $f_{\rm d}(\lambda)$ and the anisotropically scattered (and thus polarized) nuclear light $f_{\rm s}(\lambda)$. The original source for both components is the intrinsic nuclear spectrum $f_0(\lambda)$. In general, due to different aspect angles, $f_0(\lambda)$ can be different for the direct light and the scattered light, and $f_{0,\rm d}$ and $f_{0,\rm s}$ need not be identical. The intrinsic spectrum is modified by extinction $\mathcal{E}(\lambda)$ and in the case of the scattered radiation also by the function $\mathcal{S}(\lambda)$ describing the properties of the scattering medium and geometry. Thus with these assumptions the observed flux can be written as:

$$f_{\rm AGN} = f_{\rm d} + f_{\rm s} = f_{0,\rm d}\,\mathcal{E}_{\rm d} + f_{0,\rm s}\,\mathcal{S}\,\mathcal{E}_{\rm s}\,. \quad (1)$$

Similarly, we get for the polarized flux from the nucleus

$$p_{\rm AGN} \times f_{\rm AGN} = p_{\rm d} \times f_{\rm d} + p_{\rm s} \times f_{\rm s}\,, \quad (2)$$

where $p_{\rm d}(\lambda)$ and $p_{\rm s}(\lambda)$ describe the relative polarization for the direct and the scattered radiation. Of course, $f_{\rm d}$ and $f_{\rm s}$ in Eq. (2) can be split up further as in Eq. (1).

The quantities in Eqs. (1) and (2) derived from the observations are $f_{\rm AGN}(\lambda)$ and $p_{\rm AGN}(\lambda)$. From these, it is normally not possible to derive the wavelength dependent functions $f_{0,\rm d}$, $f_{0,\rm s}$, $\mathcal{E}_{\rm d}$, $\mathcal{E}_{\rm s}$, $\mathcal{S}$, $p_{\rm d}$ and $p_{\rm s}$. However, with some reasonable assumptions and simplifications we can split the AGN flux $f_{\rm AGN}$ and polarized flux spectrum $p_{\rm AGN} \times f_{\rm AGN}$ into a reddened ($E_{B-V} \approx 0.8 - 1.0$ mag) direct component $f_{\rm d}$, and a scattered component $f_{\rm s}$.

For this purpose we make the following assumptions:

(a) The initial emission from the nucleus is assumed to be the same for the direct light and the scattered light (i.e. $f_{0,\rm d} = f_{0,\rm s} = f_0$). This is supported by the observed broad line profiles, which are identical in total and polarized flux;

(b) The intrinsic light from the nucleus $f_0(\lambda)$ is assumed to have a spectral energy distribution similar to unreddened (unobscured) Seyfert 1 nuclei. According to Winkler (1997) the corresponding broad-band colours for f_0 are $B - V = 0.0$ and $U - B = -1.1$ or a power law index of about $\alpha = -0.7$ in the region 3500 Å to 9000 Å, where α is defined as $f(\nu) \propto \nu^{-\alpha}$ ($f(\lambda) \propto \lambda^{\alpha-2}$);

(c) For the reddening $\mathcal{E}_{\rm d}(\lambda)$ and $\mathcal{E}_{\rm s}(\lambda)$ we assume a standard interstellar reddening law (e.g. Cardelli et al. 1989). Furthermore, we assume that the extinction for both, the direct and the scattered radiation, is at least $E_{B-V} = 0.6$ mag as measured for the narrow line region;

(d) For the intrinsic polarization of the direct light we assume $p_{\rm d} = 0$. This appears justified by the fact that normal (unobscured) Seyfert 1 nuclei show little or no polarization. Furthermore, the absence of clear evidence of host galaxy interstellar polarization in the narrow lines (see Sect. 4.2.2) indicates that the polarization introduced by dichroic absorption in the host galaxy is small and can be neglected (the Galactic dust polarization has already been corrected in the $p_{\rm AGN}$-spectrum). This assumption simplifies Eq. (2), which now can be written

$$p_{\rm AGN} \times f_{\rm AGN} = p_{\rm s} \times f_{\rm s}\,. \quad (3)$$

(e) The relative polarization of the scattered light is assumed to be wavelength independent ($p_{\rm s}(\lambda) = {\rm const}$). This is a reasonable approximation for all cases where the scattering albedo is roughly wavelength independent, which is the case, e.g., if scatterings occur predominantly by electrons or predominantly by astrophysical dust particles (Zubko & Laor 2000). Of these two possibilities, dust scattering appears by far more likely since the scattering efficiency per unit mass is so

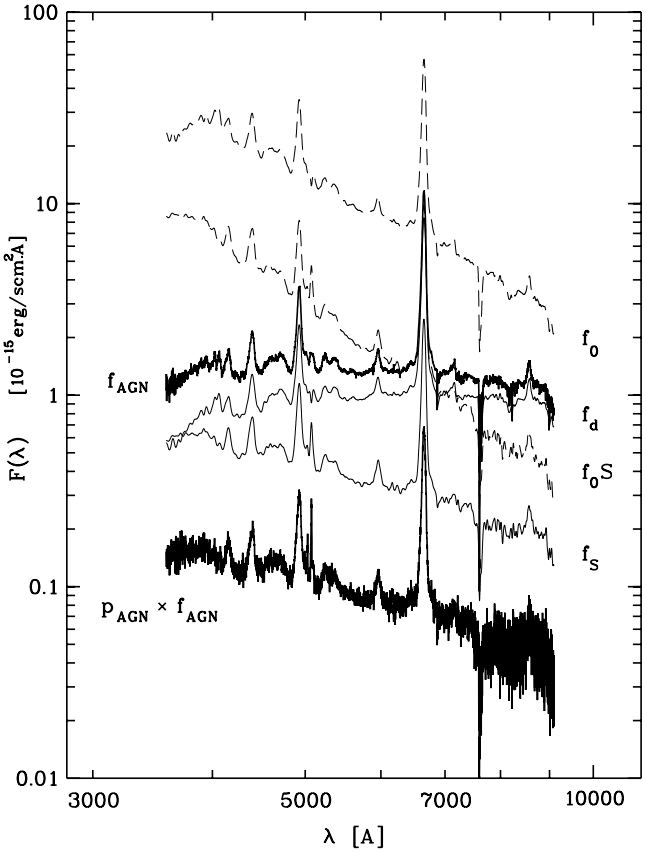

Fig. 4. Decomposition of the nuclear spectrum $f_{\rm AGN}$ into direct $f_{\rm d}$ and scattered $f_{\rm s}$ light (thin, smoothed lines) and the corresponding dereddened spectra f_0 and $f_0 \cdot \mathcal{S}$ (dashed, smoothed lines). The model adopts a polarization of $p_{\rm s} = 25\%$ for the scattered radiation, thus $f_{\rm s} = 4 \cdot p_{\rm AGN} \times f_{\rm AGN}$. The (assumed) initial spectrum with a canonical index $\alpha = -0.7$ is obtained with a dereddening of $f_{\rm d}$ by $E_{B-V} = 0.83$. Dereddening of $f_{\rm s}$ by $E_{B-V} = 0.6$ as measured for the narrow line region yields the very bluened spectrum $f_0 \cdot \mathcal{S}$ expected after optically thin dust scattering.

much greater for dust. The low efficiency of electron scattering would require an unlikely large amount of mass for the scattering region. Moreover as noted already in Sect. 4, the polarized flux $p_{\rm AGN} \times f_{\rm AGN}$ is considerably bluer than the total flux. Applying a reddening correction of $E_{B-V} = -0.6$ mag yields a spectral index of $\alpha = -1.7$ for the polarized flux. This is significantly steeper than $\alpha = -0.7$ as expected for the unobscured nucleus. We can therefore conclude that scattering is stronger for blue light than red light. Scattering by an astrophysical mixture of dust particles in the optical thin regime has a wavelength dependence of roughly $\mathcal{S}(\lambda) \propto \lambda^{-1}$ in the optical range (Zubko & Laor 2000). Therefore dust scattering can explain the blue colour of the polarized spectrum $p_{\rm AGN} \times f_{\rm AGN}$, provided the scattering opacity is small $\tau < 1$.

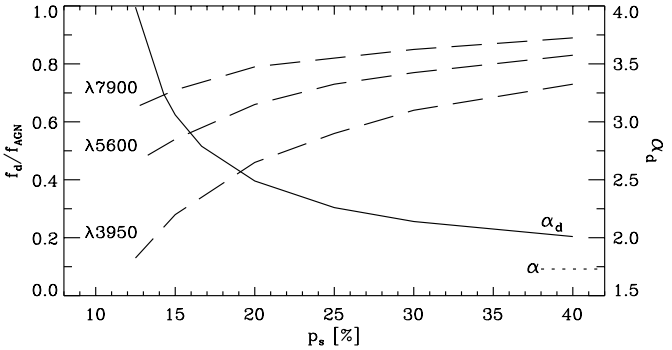

Fig. 5. The relative contribution $f_{\rm d}/f_{\rm AGN}$ at λ3950, λ5600 and λ7900 (broken lines) and spectral index $\alpha_{\rm d}$ of the direct component as a function of the adopted polarization of the scattered light $p_{\rm s}$. The observed spectral index α for the nuclear spectrum $f_{\rm AGN} = f_{\rm d} + f_{\rm s}$ is indicated at the lower right.

5.2. Separating direct and scattered light

With the assumptions made above we can estimate the ratio between scattered radiation and the total light. In the case of dust scattering, the maximum achievable polarization is about $p_{\rm s} = 40\%$ for the most favourable scattering geometry and grain properties (see e.g. Zubko & Laor 2000). On the other hand, the observed polarization provides a lower limit on $p_{\rm s}$ of 13%.

The spectral index of the direct spectrum $\alpha_{\rm d}$ depends on the adopted amount of scattered light. In any case $\alpha_{\rm d}$ is steep (i.e. red) and at least $\alpha_{\rm d} > 1.8$. The spectral index of the total (direct and scattered) light is $\alpha = 1.73$ and any subtraction of a blue scattering component makes this index larger. Thus the direct component suffers a reddening which is larger than $E_{B-V} = 0.6$ mag as measured from the narrow line region (adopting $f_{\nu,0} \propto \nu^{0.7}$). For example, if we assume that the scattered light contributes about 44% to the total nuclear light at λ3950, then the reddening of the direct light is about $E_{B-V} = 0.83$ mag, or 0.23 mag larger than the adopted reddening for the scattered light measured for the NLR (see case $p_{\rm s} = 25\%$ in Table 5).

Figure 5 illustrates the dependence of the spectral index of the direct light and the relative contribution to the total nuclear light $f_{\rm d}/f_{\rm AGN}$ (for different wavelengths) on the adopted polarization of the scattered light $p_{\rm s}$. Table 5 gives the corresponding numbers for these quantities as well as for the resulting reddening of the direct light and the initial nuclear flux f_0^{5600}.

The different models are defined by the relative polarization for the scattered light $p_{\rm s}$, which fixes the amount of scattered light via $f_{\rm s} = p_{\rm AGN} \times f_{\rm AGN}/p_{\rm s}$ and the direct spectrum $f_{\rm d} = f_{\rm AGN} - f_{\rm s}$. The spectral index for the direct spectrum $\alpha_{\rm d}$ was determined from the $f_{\rm d}$-fluxes at 3950 Å and 7900 Å. Assuming an unreddened initial core spectrum with spectral index $\alpha = -0.7$ yields the total reddening (including the extinction in the Milky Way and in the host galaxy) for the transmitted spectrum according to $E_{B-V} = (\alpha_{\rm d} + 0.7)/3.575$ (using a standard interstellar

Table 5. The relative contribution f_d/f_{AGN} at λ3950, λ5600 and λ7900, the spectral index α_d, extinction $E(B-V)$ and initial flux f_0^{5600} of the direct component as function of the adopted polarization of the scattered light p_s. Values for f_{AGN} and p_{AGN} are given at the bottom of the table. Units for f_{AGN} and f_0^{5600} are 10^{-15} erg/(cm^2 s Å).

p_s	f_d/f_{AGN}			α_d	E_{B-V}	f_0^{5600}
[%]	3950	5600	7900		mag	10^{-15}
40	0.73	0.83	0.89	2.01	0.76	19.0*
30	0.64	0.77	0.85	2.14	0.79	19.6*
25	0.56	0.73	0.82	2.26	0.83	20.3*
20	0.46	0.66	0.79	2.49	0.89	22.0*
15	0.28	0.54	0.71	3.06	1.05	28.9*
12.5	0.13	0.46	0.65	3.99	1.31	50.6*
f_{AGN}	2.90*	2.63*	2.40*			
p_{AGN}	10.8%	6.8%	4.4%			

*: Multiplied by an aperture correction factor of 2 in order to account for the light losses on the slit. These values are useful for estimates on the intrinsic and apparent nuclear luminosity.

extinction law). The initial flux at λ5600 emitted by the AGN along the line of sight f_0^{5600} follows then from the extinction and f_d. This value includes an aperture correction accounting for the light losses on the narrow slit used in our observations (see Sect. 3.1).

5.3. Likely parameters for F51

Even with all the assumptions made above it is not possible to determine uniquely the various contributions to the observed total nuclear spectrum and the corresponding polarized flux. However, the range of possible values can be constrained significantly and likely values can be given. Table 5 provides an overview about the possible parameter range and Fig. 4 illustrates the spectral decomposition for the typical value $p_s = 25\%$. The parameters for this case differ only slightly when compared to $p_s = 20\%$ or 30%. Adopting a lower p_s-value seems to be unlikely, because this would imply that the direct spectrum shows a unrealistically high reddening so that the observed flux in the blue spectral region would be almost only due to scattered light.

In the $p_s = 25\%$ model the initial flux of the core at λ5600 is $f_0^{\lambda 5600} \approx 20\ 10^{-15}$erg/(cm^2 s Å), from which only about a tenth is directly transmitted through the dust in the host galaxy and the Milky Way ($E_{B-V} = 0.83$). Correcting the scattered spectrum for interstellar reddening $E_{B-V} = 0.60$ yields a ratio of $f_0 \cdot \mathcal{S}/f_0 = 0.26$ between scattered light and initial light. This ratio depends for given wavelengths only little on the adopted model parameters. For $p_s = 30\%$, 20% or 15% and at λ5600 the ratio $f_0 \cdot \mathcal{S}/f_0$ is 0.22, 0.30 or 0.30, respectively. As the single scattering albedo for optically thin dust scatterings is between 50 and 60%, about half (or more) of the initial light from the AGN is scattered by dust in F51. For this rough estimate we assumed that the initial light f_0 and the scattered light $f_0 \cdot \mathcal{S}$ is emitted isotropically.

From the high scattering polarization of $p_s = 15-40\%$ we can further infer that the typical scattering angle must be in the range $45°-135°$. Lower or larger angles corresponding to forward or backward scattering situations respectively are not producing relative scattering polarizations in excess of $p_s \approx 15\%$ (e.g. Zubko & Laor 2000). The high p_s indicates also that the polarization is not strongly lowered by geometric canceling of the scattering polarization. This means that the scattering occur in a well defined sector having a half opening angle of not more than about 45°.

6. Discussion

6.1. Comparison with related objects

F51 is not unique among broad line Seyfert 1 galaxies in having a high scattering polarization with a polarization increasing towards the blue. Other examples are Mrk 231, Mrk 376, Mrk 486 and Mrk 704 (e.g. Schmidt & Miller 1985; Goodrich & Miller 1994; Smith et al. 1995, 1997). In all these systems the observed polarization has been explained by a combination of light scattered by dust and strongly reddened direct light from the nucleus. However, in contrast to F51 it has generally not been possible to separate the observed polarization into distinct components and to identify the scattering medium as optically thin dust.

A significant difference of the polarization observed in some of the objects quoted above is the behaviour of the polarized line flux. In contrast to our results for F51, complex polarization structures through the Hα and Hβ line profiles have been found in the high-p Seyfert 1 galaxies Mrk 231, Mrk 486 and Mrk 704 (Goodrich & Miller 1994; Smith et al. 1995, 1997). This may indicate that in these objects at least some polarization originates from scattering within or close to the BLR, or that large scale gas motions are present. As pointed out above, for F51 we found the broad line profiles of Hα and Hβ practically indistinguishable in total and polarized flux, including subtle line asymmetries.

An additional but very small polarization component in the Hα line wings can be recognized in our high quality data (Fig. 1) as a small position angle rotation over the Hα profile. Such weak polarization features in the Hα line wings are often present in high quality data of Seyfert 1 and broad line radio galaxies (Goodrich & Miller 1994; Corbett et al. 1998; Martel 1998; Young et al. 1999; Schmid et al. 2000). They are probably caused by electron scattering within or close to the BLR. In F51 this line wing component is about 20 times smaller than the overall polarization level, and the position angle of the line wing components is polarimetrically orthogonal (i.e. $\Delta\theta = \pm 45°$) to the main polarization component. It is beyond the scope of this paper to investigate the nature of

the small line wing polarization, which seems to be generic for AGN. Therefore we plotted in Fig. 2 only polarized flux and percentage polarization representing the main polarization component free from the very small "orthogonal" line wing component.

An important result for F51 is that the polarization spectrum of the nucleus and the BLR are (apart from the bluening) exact copies of the intensity spectrum. This seems to indicate that F51 differs from other AGN by the fact that for F51 we see exactly the same velocity structure of the line emitting medium along the direct line of sight to the core as well as along the direction to the scattering medium.

6.2. A tentative model of the F51 core

If our decomposition of the observed intrinsic spectrum of the F51 core into (essentially) unpolarized reddened direct light and linearly polarized bluer light, scattered by optically thin dust is correct, F51 provides the rare opportunity to observe the same Seyfert core from two different directions. Therefore, it is important to derive, or at least to constrain, the aspect angles under which the core of F51 is seen in direct and in scattered light.

As pointed out above, F51 combines some properties of a Seyfert 1 nucleus (BLR lines, power law continuum) with some typical Seyfert 2 properties (high polarization, strong reddening of the core). In the framework of the standard unified AGN model such a behaviour is explained most easily by assuming that the line of sight of the direct light passes very close to the inner boundary (or through the outer atmosphere) of a circumnuclear dust torus. Such dust tori are well know to exist in AGN and the mid-IR flux of F51 listed in the IRAS catalog strongly supports the presence of such a torus in F51. Assuming typical torus models (see e.g. Pier & Krolik 1993; Granato & Danese 1994; Efstathiou & Rowan-Robinson 1995) the above assumption would mean an inclination angle of the direct beam of the order 45°.

At a first glance it is tempting to assume that the observed polarized flux is nuclear light backscattered from the illuminated (and unobscured) opposite inner wall of the torus. Since for this light the scattering angle is near 90°, a high polarization is to be expected. The assumption would also provide a natural explanation for the identical BLR profiles observed in the direct and scattered light, since the aspect angle of the initial beam (before scattering) would be again about 45°, as in the case of the direct beam. However, this assumption has the following serious problem: from the above analysis we had to conclude that the ratio between scattered $f_0 \cdot \mathcal{S}$ and direct light f_0 (before reddening losses) has to be of the order $f_0\mathcal{S}/f_0 \approx 0.25$. A much smaller value would be incompatible with the observed high polarization of the total light and the moderate intrinsic reddening of the direct light, except if the extinction by the torus dust would follow a very unusual, essentially color independent, dust extinction law, which we regard as unlikely. With reasonable scattering efficiencies such a high percentage of scattered light can be achieved only if about 50% of the flux radiated from the core into a 2π solid angle is intersected by scattering dust. On the other hand, with plausible torus geometries and the assumed inclination angle for the direct beam at most a few per cent of the light of the core will be scattered in the visible part of the torus inner wall. Another problem with scattering from this region of the torus would be the optical thickness of the scattering layer which would decrease the scattering efficiency and the bluening effect.

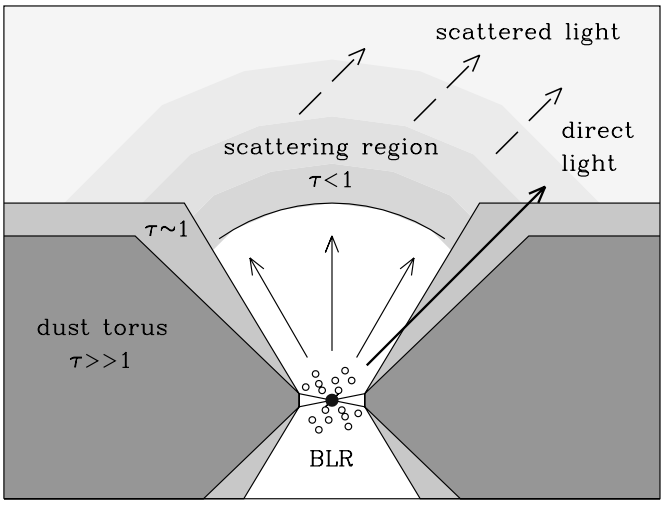

Fig. 6. Schematic scattering geometry suggested for F51. The black dot in the middle of the BLR clouds is the continuum source.

Therefore, on the basis of the inferred relatively large fraction of the scattered radiation, we conclude that the scattering must be produced by dust distributed over the whole volume inside or above the torus, with a sufficient total cross section in order to cover a large fraction of the 2π solid angle. The suggested scattering geometry is illustrated schematically in Fig. 6. The dust in the main scattering region could be contained either in an outflowing plasma which is evaporating from the torus walls, or it could be host galaxy dust located above (and below) the torus. As pointed out, e.g., by Wolf & Henning (1999) such dust configurations can produce polarized light very efficiently.

If the dust is distributed over the whole space above the torus the aspect angle of the core (i.e. of the continuum source and BLR) as seen from the dust scattering clouds will be different than in the case of light scattered off the torus wall, and it will also be different from the aspect angle of the direct light. On average the scattered light will now originate from the source in a direction approximately perpendicular to the accretion disk plane, i.e. at an angle of ≈45° relative to the direct beam (e.g. Fig. 6). Therefore, we should see in general a different radial velocity field and thus different BLR line profiles for the direct and the scattered radiation. Identical lines profiles

are only expected for cases with an isotropic velocity field of the BLR emitting matter (or certain very special and unrealistic velocity distributions).

Since the observed line profiles were found to be indistinguishable, it appears difficult to avoid the conclusion that the BLR velocity field of F51 is essentially spherically symmetric. This seems to exclude (for this AGN) models where the broad lines are produced in a disk-like configuration of BLR clouds. On the other hand the observations would be compatible with BLR models assuming the lines being formed in the bloated atmospheres or winds of a dense star cluster ionized by the central continuum source.

Type 1 AGN with a scattering geometry like F51 are rare. Unlike in F51, in most AGN an important fraction of scattering polarization seems to orignate from scattering regions located close to or within the BLR. Therefore, the profiles of the scattered broad lines are distorted and depend strongly on the exact location and dynamics of the scattering region. For the investigation of aspect-dependent properties of the BLR, it is therefore important to study type 1 systems like F51 with a rather well defined scattering region located far away from the BLR. This offers the unique opportunity to investigate the BLR velocity field from different aspect angles as described in this work. Therefore, it would be of great interest to see if the evidence for a spherically symmetric BLR velocity field found in F51 is restricted to this object or if similar evidence can be found for other AGN.

Acknowledgements. It is a pleasure to thank Andreas Kaufer and Chris Lidman for their helpful support at the telescope. An anonymous referee made several very competent remarks and constructive suggestions which improved the paper. This research has been supported by the Sonderforschungsbereich SFB 439.

References

Allen, D. A. 1979, MNRAS, 186, 1P
Angel, J. R. P., & Stockman, H. S. 1980, ARA&A, 8, 321
Antonucci, R. 1993, ARA&A, 31, 473
Antonucci, R., & Miller, J. 1985, ApJ, 297, 621
Appenzeller, I., Fricke, K., Fürtig, W., et al. 1998, ESO-Messenger, 94, 1
Brindle, C., Hough, J. H., Bailey, J. A., et al. 1990a, MNRAS, 244, 577
Brindle, C., Hough, J. H., Bailey, J. A., et al. 1990b, MNRAS, 244, 604
Cardelli, J. A., Clayton, G. C., & Mathis, J. S. 1989, ApJ, 345, 245
Cohen, M. H., Ogle, P. M., Tran, H. D., Goodrich, R. W., & Miller, J. S. 1999, AJ, 118, 1963
Corbett, E. A., Robinson, A., Axon, D. J., Young, S., & Hough, J. H. 1998, MNRAS, 296, 721
Efstathiou, A., & Rowan-Robinson, M. 1995, MNRAS, 273, 649
Goodrich, R. W., & Miller, J. S. 1994, ApJ, 434, 82
Granato, G. L., & Danese, L. 1994, MNRAS, 268, 235
Hamuy, M., & Maza, J. 1989, AJ, 97, 720
Jenkins, E. B. 1978, ApJ, 219, 845
Malkan, M. A. 1983, ApJ, 264, L1
Malkan, M. A., Gorjian, V., & Tam, R. 1998, ApJS, 117, 25
Martel, A. R. 1998, ApJ, 508, 657
Martin, P. G., Thompson, I. B., Maza, J., Angel, & J. R. P. 1983, ApJ, 266, 470
Mathewson, D. S., & Ford, V. L. 1970, Mem. R. Astron. Soc., 74, 139
Mathewson, D. S., Ford, V. L., Klare, G., Neckel, T., & Krautter, J. 1978, Bull. d. Inf. CDS Strasbourg, 15, 125
Miller, J. S., & Goodrich, R. 1990, ApJ, 355, 456
Morris, S. L., & Ward, M. J. 1988, MNRAS, 230, 639
Pier, E., & Krolik, J. H. 1993, ApJ, 418, 673
Serkowski, K. 1970, ApJ, 160, 1083
Serkowski, K., Mathewson, D. S., & Ford, V. L. 1975, ApJ, 196, 261
Schlegel, D. J., Finkbeiner, D. P., & Davis, M. 1998, ApJ, 500, 525
Schmid, H. M., Appenzeller, I., Camenzind, M., et al. 2000, Proc. of SPIE, 4005, 264
Schmidt, G. D., & Miller, J. S. 1985, ApJ, 290, 517
Smith, P. S., Schmidt, G. D., Allen, R. G., & Angel, J. R. P. 1995, ApJ, 444, 146
Smith, P. S., Schmidt, G. D., Allen, R. G., & Hines, D. C. 1997, ApJ, 488, 202
Terlevich, E., Diaz, A. I., & Terlevich, R. 1990, MNRAS, 242, 271
Thompson, I. B., & Martin, P. G. 1988, ApJ, 330, 121
Tinbergen, J., & Rutten, R. 1997, Measuring polarization with ISIS, Users' manual, The Isaac Newton Group of Telescopes, `http://www.ing.iac.es/`
Tsvetanov, Z. I., & Yancoulova, I. M. 1989, MNRAS, 237, 707
West, R. M., Danks, A. C., & Alcaino, G. 1978, A&A, 65, 151
Winkler, H. 1992, MNRAS, 257, 677
Winkler, H. 1997, MNRAS, 292, 273
Wolf, S., & Henning, Th. 1999, A&A, 341, 675
Young, S., Corbett, E. A., Giannuzzo, M. E., et al. 1999, MNRAS, 303, 227
Zorec, J., & Briot, D. 1991, A&A, 245, 150
Zubko, V. G., & Laor, A. 2000, ApJS, 128, 245